Post-adaptive optics speckle imaging in the visible

Jérémy Deguignet[1,2], Marcel Carbillet[1], Éric Aristidi[1]

[1]: UMR 7293 Lagrange (Université de Nice Sophia-Antipolis/CNRS/Observatoire de la Côte d'Azur), Parc Valrose, 06100 Nice, France
[2]: Master Imagerie et Modélisation Astrophysique et Géophysique, Espace et Environnement (Université de Nice Sophia-Antipolis), Parc Valrose, 06100 Nice, France

Abstract In the visible domain, turbulence is very fast and strong, and adaptive optics (AO) systems cannot provide full correction. In this context one can wonder whether deconvolution techniques are still that relevant, or whether it would be more interesting to work directly on short-exposure images by means of speckle methods used on partially corrected images. The purpose of this work is hence to make a first comparison, by means of numerical simulations of binary star post-AO images, between: (i) deconvolution methods applied to a long-exposure image, and (ii) speckle methods applied to a set of short-exposure images.

Data simulation

The data were simulated by means of the Software Package CAOS [10], part of the CAOS Problem-Solving Environment (PSE) [9, 12, 15], and considering the 1.54-m telescope MéO (plateau de Calern, France) of the Observatoire de la Côte d'Azur, equipped with the ODISSEE AO system. In order to simulate different regimes of correction, we consider here a (rather pessimistic) Fried parameter of 5 cm (at 500 nm), an outer-scale of turbulence of 25 m, and a partial correction on the first 44 Zernike modes (8^{th} radial order) of the incident perturbated wavefronts. The test-object considered is a binary star of separation 0.″24 (i.e. $\sim$2.5 λ/D at the observing wavelength, λ=700 nm, and 16 px with the chosen pixel scale, 0.″015), and a magnitude difference between the two components of 1. Examples of short-exposure and long-exposure images obtained are shown below (using a square-root scale), where each image corresponds to a given percentage of correction (from left to right: 75%, 80%, 85%, 87%, 89%, 90%, 95%, 100%, resulting in the following average Strehl ratio values: 0.024, 0.036, 0.059, 0.075, 0.095, 0.106, 0.170, 0.205). A thousand independent realizations is simulated, resulting in a set of 1000 short-exposure images in one hand, and 1 single integrated long-exposure image in the other hand, for each correction case. The same is done for the estimates of the point-spread function (PSF, corresponding to the subsequent observation of a nearby reference star, simulated here by means of a different random seed).

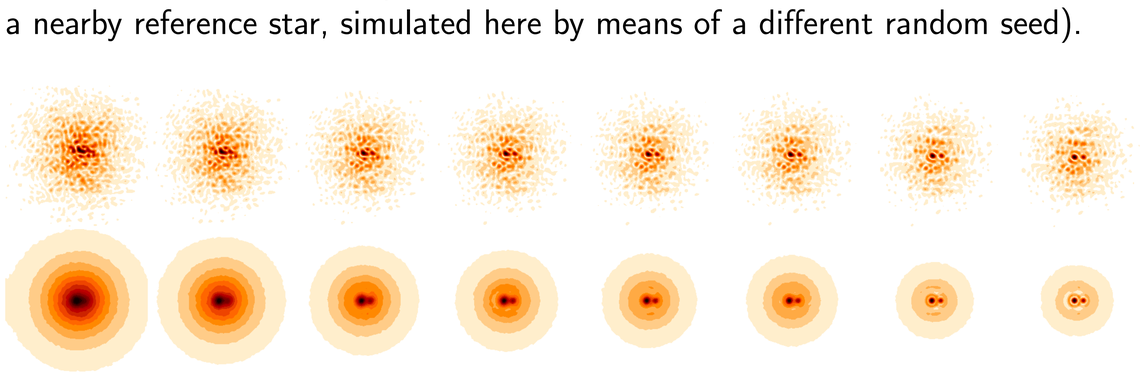

Short-exposure imaging: Knox-Thompson technique

Speckle techniques were introduced in the early 1970's [1] to attain diffraction-limited resolution by means of post-processing of short-exposure images. Denoting as $O(\mathbf{x})$ the ideal angular brightness distribution of the observed object, and $I(\mathbf{x})$ the turbulence-blurred images of this object by a telescope, the following relation (where $\langle\rangle$ is an ensemble average and $S(\mathbf{x})$ the atmosphere$\oplus$telescope PSF):

$$\langle|\hat{I}(\mathbf{u})|^2\rangle \;=\; |\hat{O}(\mathbf{u})|^2 \,\langle|\hat{S}(\mathbf{u})|^2\rangle \;, \qquad (1)$$

makes it possible to estimate the object power spectrum $|\hat{O}(\mathbf{u})|^2$. The method cannot provide the exact object since the phase $\phi(\mathbf{u})$ of its Fourier transform is lost. Knox and Thompson hence proposed [4] a technique (KT) to estimate $\phi(\mathbf{u})$ by computing the following cross-spectrum:

$$W_{\text{KT}}(\mathbf{u}) = \langle \hat{I}(\mathbf{u}).\hat{I}(\mathbf{u}+\delta\mathbf{u})^{*}\rangle \;, \qquad (2)$$

where $\delta\mathbf{u}$ is a small spectral lag in the Fourier plane. The phase of $W_{\text{KT}}(\mathbf{u})$ is equal to the derivative of $\phi(\mathbf{u})$. A numerical integration provides $\phi(\mathbf{u})$, and the diffraction-limited object $O(\mathbf{x})$ is then computed by inverse Fourier transform. The figure hereafter shows, from left to right: the object power spectrum $|\hat{O}(\mathbf{u})|^2$, the phase of $W_{\text{KT}}(\mathbf{u})$, and the reconstructed object $O(\mathbf{x})$, for the 0.024 Strehl case.

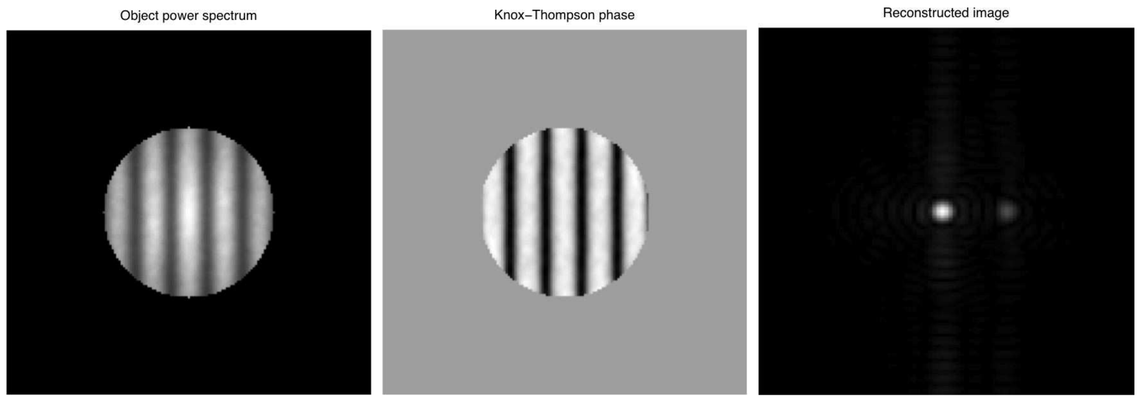

Long-exposure imaging: Lucy-Richardson deconvolution

The classical Lucy-Richardson (LR) method [2, 3] is described by the following algorithm, implemented within the Software Package AIRY [8, 13, 16] (part of the CAOS PSE as well), and used in these tests with 1000 iterations.

Choose the starting point $\mathbf{f}^{(0)} \geq 0$
FOR $k = 0, 1, 2, \ldots$ COMPUTE:

$$\mathbf{f}^{(k+1)} = \mathbf{f}^{(k)} A^{T} \frac{\mathbf{g}}{A\mathbf{f}^{(k)} + \mathbf{b}}$$

END

(Where $\mathbf{f}^{(k)}$ is the vector describing the object reconstructed at the k^{th} iteration, $\mathbf{g}$ the acquired image to be deconvolved, $\mathbf{b}$ an estimate of the sky background, and A the imaging matrix given by $A\mathbf{f} = \mathbf{K} \star \mathbf{f}$, with $\star$ the convolution operator and $\mathbf{K}$ an estimate of the normalized PSF.)

Quantitative comparison

Next figure shows the result of the comparison between the performance obtained with KT and LR on the reconstruction of the intensity ratio α between the two components of the considered binary, in function of the Strehl ratio of the images and the PSFs. The error is computed by aperture photometry of dimension $\sim\lambda/D$.

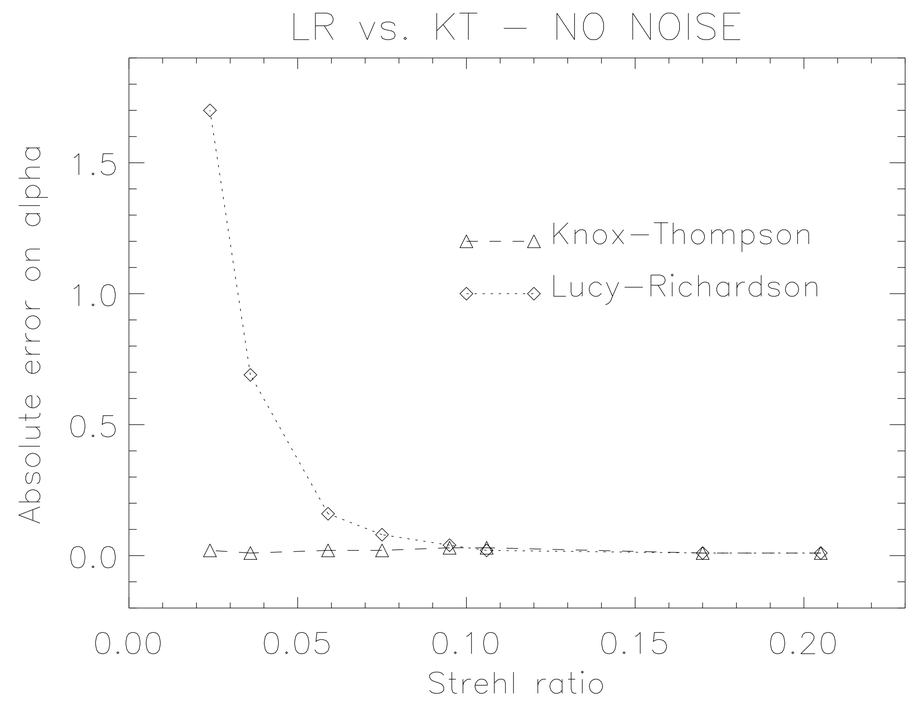

Conclusion and perspectives

The results shown here before clearly suggest that while KT seems not to be affected at all by the partial AO correction, it is definitely the case for LR, at least when the Strehl ratio reach values lower or of the order of 10%. In fact, the two methods perform identically for Strehl ratio values above 10%, but the LR performance becomes worse as the Strehl ratio value decreases from this critical value. It is important to emphasize that the present results were obtained in complete missing of any kind of noise. Consideration of the latter (with the due differences between the two observing strategies) is the next step for this study.
Extended objects instead of binaries (the simplest object from the point of view of imaging) will also be considered. As a consequence, the bispectrum method [5] will be implemented, and Lucky imaging methods [14] will be studied as well. Another extension of this work will concern the comparison of reference-free methods, both for the long-exposure observing strategy side [11] and the short-exposure one [6, 7].

References

[1] A. Labeyrie, A&A **6**, 85 (1970).
[2] W. H. Richardson, J. Opt. Soc. Am. **62**, 55 (1972).
[3] L. B. Lucy, Astron. J. **79**, 745 (1974).
[4] K. T. Knox & B. J. Thompson, Astrophys. J. **193**, L45 (1974).
[5] G. Weigelt, Opt. Commun. **21**, 55 (1977).
[6] É. Aristidi et al., A&A Suppl. Ser. **125**, 139 (1997).
[7] M. Carbillet et al., A&A Suppl. Ser. **127**, 569 (1998).
[8] S. Corriea et al., A&A **387** (2), 733 (2002).
[9] M. Carbillet et al., SPIE Proc. **5490** (2), 550 (2004).
[10] M. Carbillet et al., MNRAS **356** (4), 1263 (2005).
[11] G. Desiderà & M. Carbillet, A&A **507** (3), 1759 (2009).
[12] M. Carbillet et al., SPIE Proc. **7736**, 773644 (2010).
[13] A. La Camera et al., SPIE Proc. **8445**, 84453E (2012).
[14] C. D. Mackay et al., SPIE Proc. **8446**, 844672 (2012).
[15] http://lagrange.oca.eu/caos (as on November 2014).
[16] http://www.airyproject.eu (as on November 2014).

N.B.: The Software Package AIRY and the Software Package CAOS can be freely downloaded from http://lagrange.oca.eu/caos.